Investigating pipeline–soil interaction under axial–lateral relative movements in sand

Nasser Daiyan, Shawn Kenny, Ryan Phillips, and Radu Popescu

Abstract: This paper presents results from an experimental and numerical study on the axial–lateral interaction of pipes with dense sand. A series of centrifuge tests were conducted, with a rigid pipeline displaced in the horizontal plane in a cohesionless test bed. The relative pipe–soil interaction included axial, lateral, and oblique loading events. A three-dimensional continuum finite element model was developed using ABAQUS/Standard (Hibbitt et al. 2005) software. The numerical model was calibrated against experimental results. A parametric study was conducted, using the calibrated finite element model to extend the investigations. The ultimate axial and lateral soil loading was found to be dependent on the angle of attack for relative movement between the pipe and soil. Two different failure mechanisms were observed for axial–lateral pipeline–soil interaction. This study confirms and improves on a two-part failure criterion that accounts for axial–lateral coupling during oblique soil loading events on buried pipelines.

Key words: buried pipeline, pipeline–soil interaction, cohesionless, sand, centrifuge tests, numerical modeling, oblique loading.

Résumé : Cet article présente les résultats d'une étude expérimentale et numérique sur l'interaction axiale–latérale entre des tuyaux et du sable dense. Une série d'essais en centrifuge ont été réalisés sur un tuyau rigide en déplacement sur le plan horizontal dans un sol sans cohésion. L'interaction relative tuyau–sol comprend des chargements axiaux, latéraux et obliques. Un modèle par éléments finis en trois dimensions continues a été développé à l'aide du logiciel ABAQUS/Standard (Hibbitt et al. 2005). Le modèle numérique a été calibré avec les résultats expérimentaux. Une étude paramétrique à été réalisée avec le modèle par éléments finis calibré dans le but de poursuivre les investigations. La charge ultime axiale et latérale du sol s'est révélée être dépendante de l'angle d'attaque du mouvement relatif entre le tuyau et le sol. Deux mécanismes de rupture différents ont été observés lors de l'interaction axiale–latérale tuyau–sol. Cette étude confirme et améliore un critère de rupture en deux parties qui considère le couplage axial–latéral durant le chargement oblique du sol comportant des tuyaux enfouis.

Mots-clés : tuyau enfoui, interaction tuyau–sol, sans cohésion, sable, essais en centrifuge, modélisation numérique, chargement oblique.

[Traduit par la Rédaction]

Introduction

In the oil and gas industry, energy pipeline systems are critical transportation elements for the transmission of hydrocarbon products over long distances. In Canada, more than 580 000 km of pipelines deliver natural gas and petroleum products from field development areas to market (www.cepa.com). One of the challenges in buried pipeline design is the effect of geohazards on the mechanical response and integrity. Permanent ground deformations caused by geohazards, such as slope movements, landslides, seismic faulting, and subsidence, are imposed on segments of the pipeline system, with other sections restrained. The relative displacement between the buried pipeline and surrounding soil will impose geotechnical loads onto the pipe. This will increase the level of stress and strain in the pipeline, which may affect pipeline operations and mechanical integrity. A report of the European Gas Pipeline Incident Data Group (European Gas Pipeline Incident Data Group 2005) has indicated that ground movement represents the fourth major cause of gas pipeline failures where almost half of the incidents resulted in pipe rupture. Advancement of the understanding of pipe–soil interaction will lead to improved engineering designs, reduced uncertainty, improved economy, and greater safety for the oil and gas pipeline industry.

Engineering guidelines (e.g., Honegger and Nyman 2004) provide an engineering model for the analysis of pipeline–soil interaction events, with structural beam elements for the pipe and spring elements for the soil. Soil behavior is modeled using discrete springs in three orthogonal (axial, lateral, and vertical) directions. The general form of the load–displacement relations for these springs can be expressed as

$$[1] \qquad T = f(x), \quad P = g(y), \quad Q = h(z)$$

where T, P, and Q are soil forces applied to the unit length of pipelines, and x, y, and z are relative displacements between

N. Daiyan and S. Kenny. Box 59, Faculty of Engineering and Applied Science, Memorial University, St. John's, NL A1B 3X5, Canada.
R. Phillips. C-CORE, Captain Robert A. Bartlett Building, Morrissey Road, St. John's, NL A1B 3X5, Canada.
R. Popescu. URS Corporation, 510 Carnegie Center, Princeton, NJ 08540, USA.

Corresponding author: N. Daiyan (e-mail: ndaiyan@mun.ca).

pipe and soil in longitudinal, lateral (horizontal), and vertical directions, respectively.

These nonlinear load–displacement relationships are generally defined by bilinear or hyperbolic functions (e.g., American Lifelines Alliance 2001; Honegger and Nyman 2004). The soil spring parameters include the ultimate load and relative soil displacement at ultimate load for each orthogonal loading axes. Theoretical, numerical, and experimental investigations have been conducted on buried pipelines and analogue systems (e.g., piles, anchor plates) to define the soil load–displacement relationships.

The load–displacement relationships for the three orthogonal soil springs are usually considered independent and without coupling. A number of experimental (e.g., Hsu et al. 2006), theoretical (e.g., Cocchetti et al. 2009), and numerical (e.g., Phillips et al. 2004) studies have been conducted to investigate the pipe–soil interaction during an oblique or three-dimensional pipe–soil relative movement. Also, there are several studies investigating foundations or buried structures under combined loading, which include Taiebat and Carter (2000) on shallow foundations, Martin and Houlsby (2000) on spud-can foundations, and Aubeny et al. (2003) on suction caissons.

Phillips et al. (2004) investigated the axial–lateral pipe–soil interaction in clay and showed that the axial soil load increased during oblique pipeline–soil interaction events for low angles of attack. Also, some studies (e.g., Cocchetti et al. 2009; Nyman 1984) have indicated the importance of lateral–vertical pipe–soil interaction. Cocchetti et al. (2009) have shown that the downward movement of pipe increases the lateral soil restraint on the pipeline. None of these coupling effects are considered in the current state of practice. Therefore, more investigations on complex loading conditions are needed to enhance the numerical tools and engineering guidelines that are used to assess the pipeline's response in a continuum pipe–soil interaction event. This study is focused on pipe–soil interaction events in dense sand for axial, lateral, and oblique axial–lateral loading conditions.

A series of centrifuge tests have been conducted in dense sand with the test procedures and results reported. Continuum finite element model procedures were developed using ABAQUS/Standard (Hibbitt et al. 2005) and validated using the centrifuge test results. Mohr–Coulomb plasticity model, which was customized to account for progressive mobilization of shear strength of soil, was implemented in ABAQUS/Standard (Hibbitt et al. 2005). Numerical parametric studies were conducted to develop a limit load interaction curve for axial–lateral pipe–soil interaction in dense sand. The proposed interaction curve can be used to define enhanced soil springs for use in conventional structural based finite element modeling procedures simulating pipeline–soil interaction events. These conventional structural based numerical procedures are improved by accounting for axial and lateral soil load coupling effects during oblique pipeline–soil interaction events.

Review of previous studies

Unlike the simplifications used in engineering practice, the relative movement between pipelines and soil during a ground movement incident may occur in axial, lateral, and vertical directions at the same time. For instance, it is rare to have pure axial pipe–soil relative displacement without any lateral or vertical displacements. While there are many studies in the literature investigating the lateral–vertical pipe–soil interaction, there are a limited number of studies on axial–lateral pipe–soil interaction, and the authors could not find any study on axial–vertical pipe–soil interaction events.

Fig. 1. Definition of the angle of movement in horizontal plane (top view).

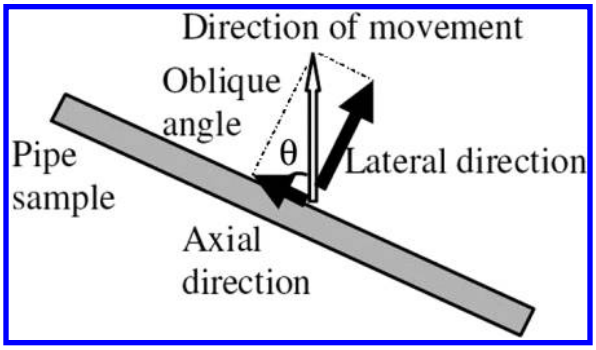

Hsu et al. (2001, 2006) investigated the axial–lateral pipe–soil interaction for shallow buried pipes in loose and dense sand. Large-scale tests were conducted for 10 different angles of movement (θ) between 0° and 90° (Fig. 1), three different pipe diameters (D), and three different pipe springline burial depth (H/D) ratios, where H is the soil cover depth to the pipe centerline. The longitudinal and lateral soil restraints on the pipe during oblique pipe–soil interaction were obtained from the vector components of the soil load on the pipe in the direction of movement.

Phillips et al. (2004) presented a parametric study using three-dimensional numerical analysis on axial–lateral pipe–soil interaction in cohesive soil. The soil failure mechanism under pure axial loading was considered to occur within a thin soil layer surrounding the pipe circumference. Although conducted in cohesive soil, this is consistent with Wijewickreme et al. (2009) full-scale test observations of a shear zone thickness of 5–12 times the mean particle size for axial pipe–soil interaction. For increasing oblique loading angles, there was corresponding increase in the axial load. At larger oblique load angles, a dominant shear failure mechanism was developed for significant lateral displacement. Phillips et al. (2004) developed an interaction diagram for combined axial–lateral loading, which is defined by the following equation:

$$[2] \qquad N_y^2 + 3N_x^2 = N_{y90}^2, \quad N_x < \alpha\pi$$

where α is the adhesion factor, N_{y90} is the lateral interaction factor under pure lateral loading, and $N_y = F_y/c_u DL$ and $N_x = F_x/c_u DL$, while F_y and F_x are the ultimate lateral and axial forces on pipe for oblique relative movement, respectively. The interaction curve accounts for two failure mechanisms during axial–lateral pipe–soil interaction events. For small oblique angles, failure occurs by sliding along the pipe–soil interface. At larger angles, the soil failure mechanism is dominated by shear and bearing. The criteria presented in Phillips et al. (2004) are independent of pipe burial depth or soil shear strength or pipe–soil interface friction angle.

Table 1. Summary of sand bed parameters.

	Angle of movement (°)[a]			
Parameters	90	0	40	70
γ' (kN/m^3)	15.68	15.66	15.66	15.7
D_r	0.825	0.82	0.82	0.83

[a]From Fig. 1.

Table 2. Summary of equivalent prototype test parameters.

Parameters	Values
Pipe diameter, D (mm)	504
Embedment depth to the pipe centerline, H (mm)	1008
Pipe length over diameter, L/D	8
Average dry density of sand, ρ (kg/m^3)	1598
Peak sand internal friction angle, φ'_{peak}(°)	43
Constant-volume friction angle, φ'_{cv}(°)	33
Pipe–soil interface friction coefficient, μ	0.44
Cohesion, c'	0

Fig. 2. Pipe section before getting buried (lateral test).

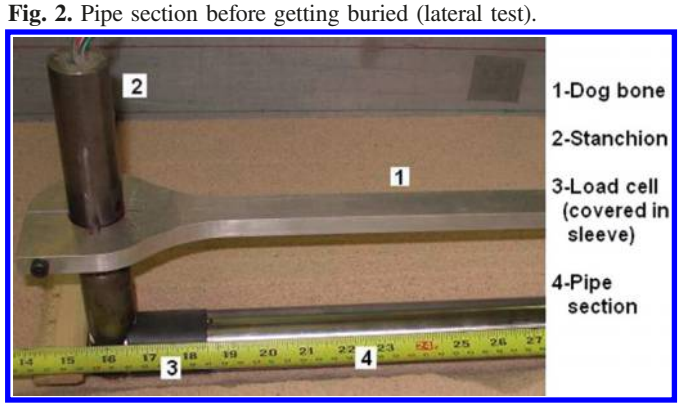

Centrifuge modeling

Centrifuge modeling is an efficient method to study gravity-dependent problems in geotechnical engineering. It has been used in several studies (e.g., Dickin 1988; Paulin et al. 1995) to investigate different aspects of pipe–soil interaction.

Four tests were conducted under a centrifugal acceleration of 12.3g and a displacement rate of 0.04 mm/s. Dry fine silica sand with specific gravity of 2.65 and with minimum and maximum void ratios of 0.60 and 0.93, respectively, were used. An average relative density of 0.82 was obtained in the four test beds using sand raining procedure. Cone penetration (CPT) tests on two different test beds confirmed the repeatability of the raining method and similarity of the sand bed at different depths. A summary of sand bed parameters for all four tests is presented in Table 1.

Direct shear tests under normal stresses of 16–65 kPa resulted in peak friction angle of 43°, constant-volume friction angle of 33°, and pipe–soil interface friction coefficient of 0.44. The model steel pipe was 41 mm in diameter, 328 mm in length (L/D = 8), and 6.35 mm in wall thickness. This provided a rigid pipe mechanical response, but the pipe weight influenced the pipe–soil interaction response. The pipe was buried to a cover depth of 61.5 mm, which corresponds to a pipe springline burial depth to pipe diameter ratio (H/D) of 2. The pipe bedding layer was 100 mm of sand, which was equivalent to 2.4 pipe diameters. The centrifuge strong box inner dimensions were 1180 mm × 940 mm × 400 mm. The prototype soil parameters are summarized in Table 2.

The buried pipe was moved in a horizontal plane using a leadscrew actuator that was connected to the two ends of the pipe through two load cells. The load cells were based on the Stroud (1971) design. Four strain-gauged longitudinal thin webs measured the axial load in compression, and two horizontal (lateral) webs measured the lateral loads.

There was cross sensitivity between axial and lateral strain gauges when lateral load was applied to the load cell, so that during pure lateral loading, strains were recorded on both lateral and axial strain gauges. Therefore, the load cells were calibrated for axial load and two sets of lateral loads with different lever arms using a coupled calibration matrix. In-air pipe loading tests were conducted to confirm the load cell measurements.

The pipe was held between the two load cells (No. 3 in Fig. 2) through a small bearing at both ends. As shown in Fig. 2, the load cells were bolted to stanchions (No. 2) and tied together by a dog-bone (No. 1) cross beam. The stanchions could move easily in the vertical direction on ball races (No. 3 in Fig. 3*b*), which were secured to the guiding plate (No. 4 in Fig. 3*b*). Vertical movement of pipe was measured by two linear variable differential transformers (LVDTs) that were secured on ball races and measured the vertical movements of two stanchions. Lateral pipe displacement was measured initially using a laser displacement sensor (No. 1 in Fig. 3*a*) on top of the horizontal actuator.

For two oblique loading cases (40° and 70°), two laser sensors (No. 2 in Fig. 3*a*) were added at a lower elevation to measure the displacement at the dog-bone level (No. 1 in Fig. 3*b*). The measured displacements were corrected for actuator compliance and are reported as estimates of displacements at the pipe's level. To account for the actuator compliance, a series of in-air tests were conducted to find the relationship between the applied load to the pipe and the corresponding stiffness of the loading system.

Crushable foam was used in front of the stanchions in axial and oblique loading tests to reduce the effect of end bearing on the axial load on the pipe. Several unloading–reloading cycles were conducted during each test to estimate the elastic response of the soil.

Numerical modeling

The numerical modeling procedures simulating pipeline–soil interaction events were developed using the finite element software package ABAQUS/Standard (Hibbitt et al. 2005). A three-dimensional continuum model (Fig. 4) was developed for the centrifuge test program at prototype scale. Dimensions of the modeled soil domain were selected to minimize boundary effects on the predicted soil load, displacement, and failure mechanisms. The bedding distance from the pipe centerline used in the numerical simulations was consistent with the centrifuge experiments (2.5D).

Eight-node continuum brick elements with reduced integration (C3D8R) for the soil domain and conventional four-node shell elements (S4R5) for the rigid pipe were used. The pipe–soil interface was simulated using the contact sur-

Fig. 3. (*a*) Plan and (*b*) elevation view of test box (oblique 40° test).

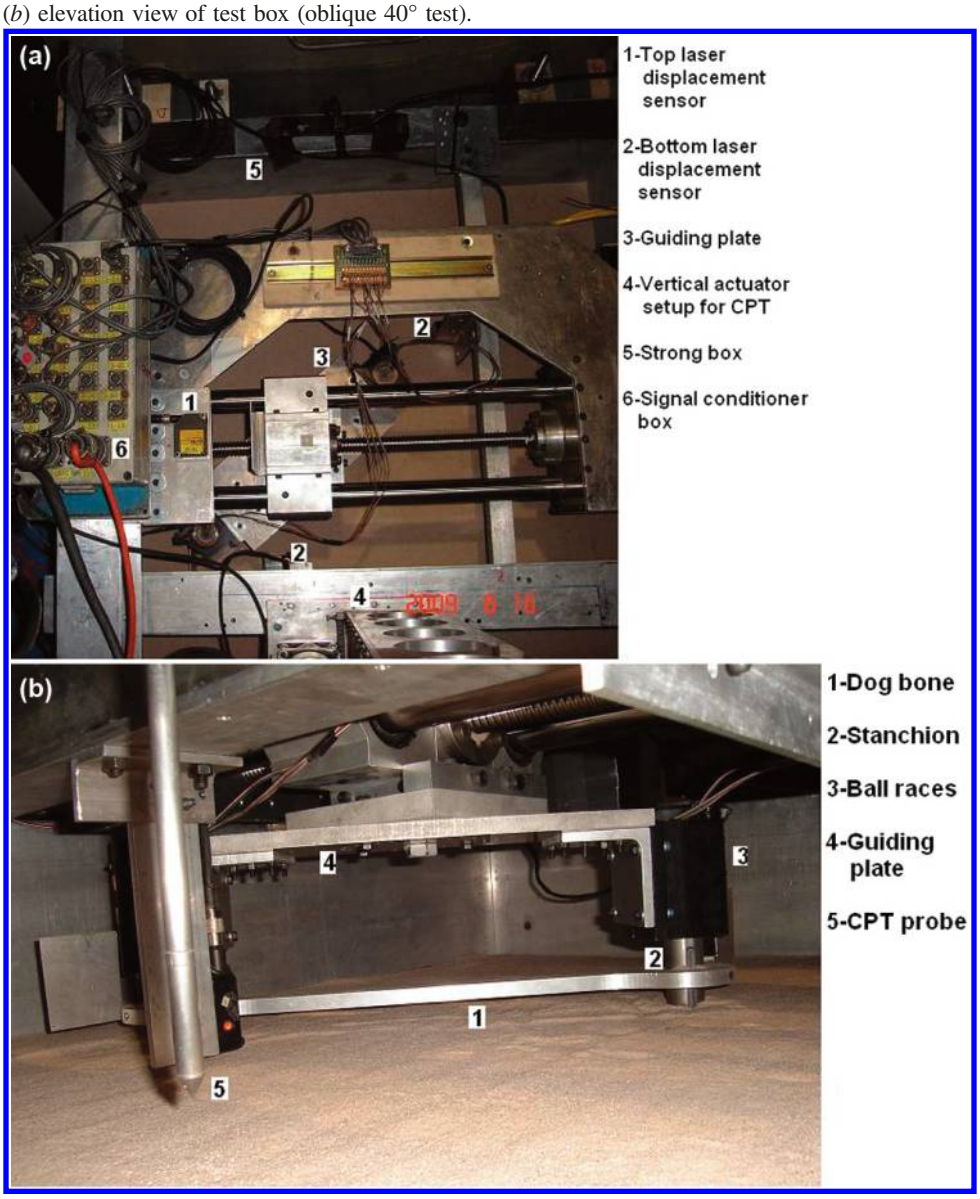

Fig. 4. The finite element model geometry.

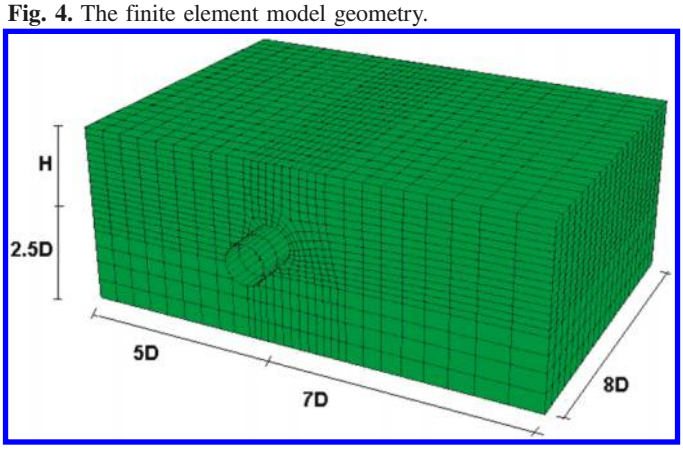

face approach implemented in ABAQUS/Standard (Hibbitt et al. 2005), which allows for separation and sliding with finite amplitude and arbitrary rotation of the contact surfaces. The Coulomb friction model was used for the frictional interface between pipe and dry sand. In this method, the friction coefficient (μ) was defined between the pipe and the soil. Sliding occurs after the shear stress on the contact surface exceeds the critical shear stress. The critical shear stress was the product of friction coefficient and contact pressure.

As the main purpose of the study was to establish the soil load–displacement relationship, a rigid pipe was used during the physical test. In the numerical model, the pipe displacement is applied to all nodes of the pipe to simulate a rigid pipe. To minimize end effects of soil loading on the pipe, only the central region having uniform stress conditions was examined. This uniform stress region was generally located within the middle third of the pipe length.

During the centrifuge modeling, the weight of the model pipe and other parts of the test apparatus (i.e., stanchions

Fig. 5. Comparison of numerical and experimental data for triaxial test: (*a*) q versus axial strain; (*b*) volumetric strain versus axial strain. FE, finite element.

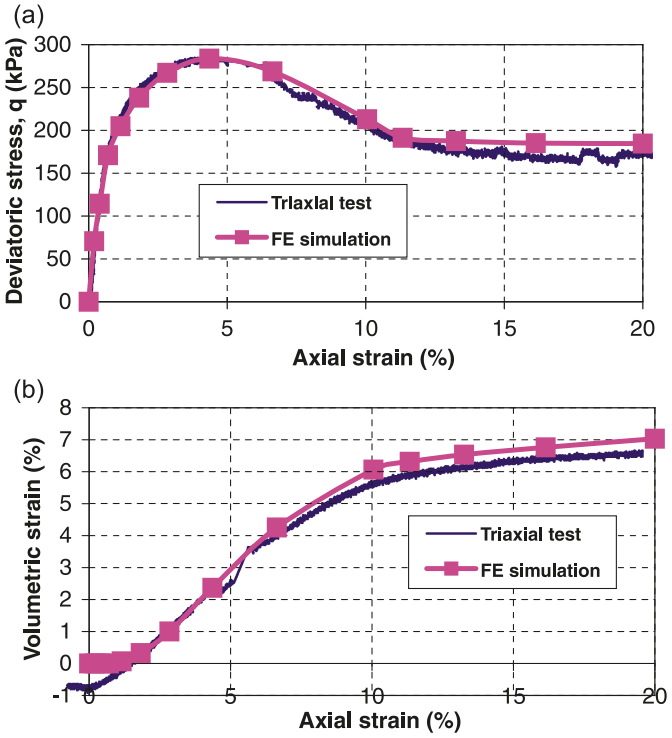

Fig. 6. Mobilization of friction and dilation angles inferred from triaxial test data.

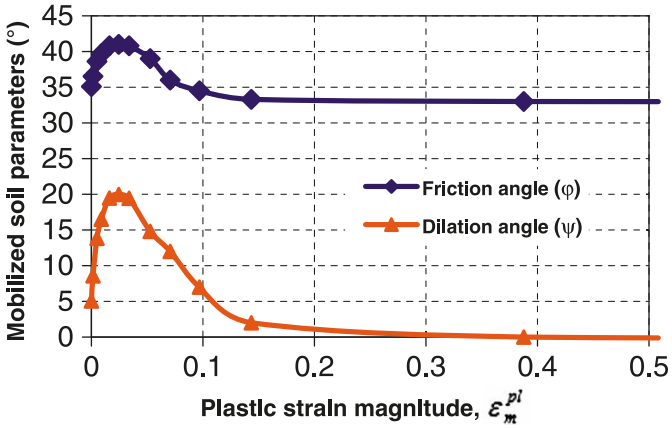

and dog bone) affected the ultimate soil restraint applied to the pipe. The effect of pipe self-weight is discussed in more detail within the next section.

The analysis was conducted in two main steps. The first step was a geostatic stress step that accounted for the effects of pipe and soil weight to determine the initial stress state in the soil. The second step was to impose the pipe displacement in the specified direction (i.e., loading angle).

The soil elastic modulus was defined using the following relation to simulate its dependence on effective confining pressure, p:

$$[3] \qquad E = E_0\left(\frac{p}{p_0}\right)^n$$

where p_0 is the reference pressure equal to the atmospheric pressure (p_0 = 100 kPa), E_0 is the soil elastic modulus at the reference pressure (E_0 = 15 000 kPa), and n is the power exponent (n = 0.5). The elastic modulus at the reference pressure (E_0) was calibrated against the triaxial test result (Fig. 5*a*). The Poisson's ratio was assumed to be 0.3. A small value of cohesion of 4 kPa was assigned to soil for numerical convergence in the pipe–soil interaction model.

The nonassociated Mohr–Coulomb plasticity model implemented in ABAQUS/Standard (Hibbitt et al. 2005) was used. Comparison of Mohr–Coulomb and Norsand as soil models by Yimsiri et al. (2004) has shown Mohr–Coulomb provides reasonable results in the case of pipe–soil interaction events. This model has also been successfully used for other studies on pipe–soil interaction involving large soil deformations (e.g., Popescu et al. 2002; Guo and Stolle 2005).

Dense sand exhibits a strain hardening and softening response with shear induced dilative behavior. Nobahar et al. (2000) described a method to estimate the progressive mobilization of soil shear strength parameters using direct shear test data. Similar procedures have been used in this study to define the soil internal friction angle and dilation angle as a function of plastic strain magnitude as a state parameter using triaxial data. The plastic strain magnitude, ε_m^{pl} was defined as

$$[4] \qquad \varepsilon_m^{pl} = \sqrt{\frac{2}{3}\boldsymbol{\varepsilon}^{pl}:\boldsymbol{\varepsilon}^{pl}}$$

where $\boldsymbol{\varepsilon}^{pl}$ is the plastic strain tensor.

Data from a triaxial test and numerical simulation is presented in Fig. 5. The soil sample was consistent with the centrifuge tests and had a 75% relative density. The effective cell pressure during the triaxial test was 70 kPa, which was based on the predicted mean effective stresses developed on the pipe surface during numerical simulations of the oblique pipe–soil interaction events.

The progressive mobilization of soil strength parameters (Fig. 6) was implemented in the finite element simulation through a user subroutine. For numerical simulation of pipe–soil interaction, the hardening rule in Fig. 6 was modified for a peak friction angle of 43°, corresponding to centrifuge test conditions (Table 2). The modification was established through analysis of the strength parameters by multiplying the ratio of $(\phi'_{peak} - \phi'_{cv})$ for two cases to $(\phi' - \phi'_{cv})$ for the relationships illustrated in Fig. 6.

Comparisons and discussions

Pure lateral loading test

Figure 7 presents the comparison between the numerical and experimental load–displacement curves during lateral pipe–soil interaction. The lateral interaction factor was defined as

$$[5] \qquad N_{qh} = \frac{P_u}{\gamma' HD}$$

where P_u is the ultimate lateral load obtained from the load–displacement curve, which was chosen as the peak load in this study.

Honegger and Nyman (2004) adopted the lateral bearing capacity factors (N_{qh}) of Hansen (1961), which are consistent with experimental results from Audibert and Nyman (1977).

Fig. 7. Numerical versus experimental curves for lateral loading test.

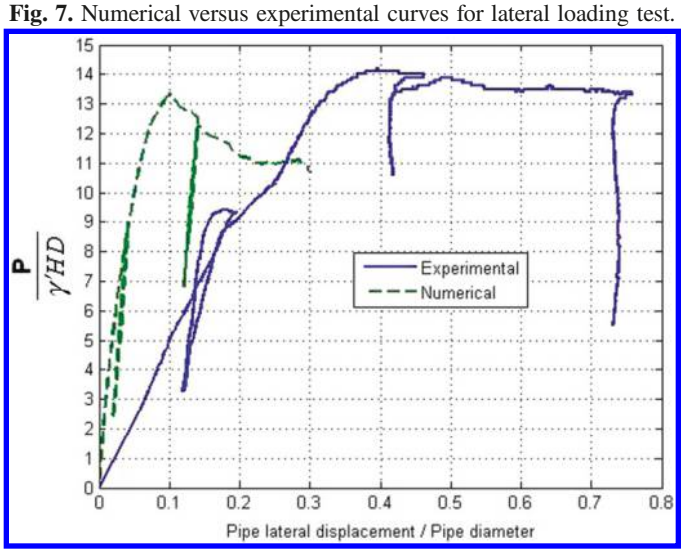

Fig. 8. Comparison of numerical analysis with ultimate lateral loads from eq. [6] (Guo and Stolle 2005).

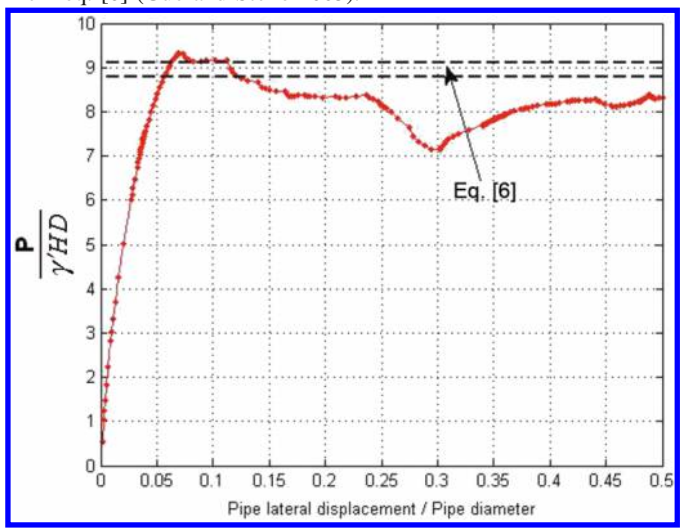

Fig. 9. Numerical versus experimental curves for axial loading test.

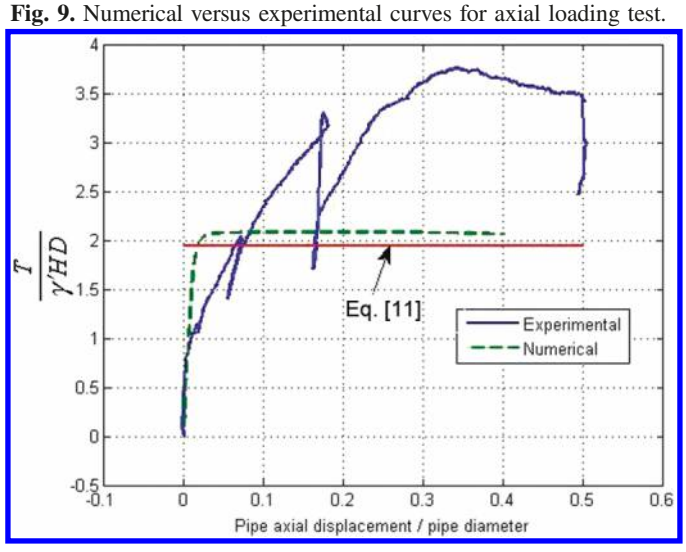

Fig. 10. Soil surface deformation after oblique 40° test.

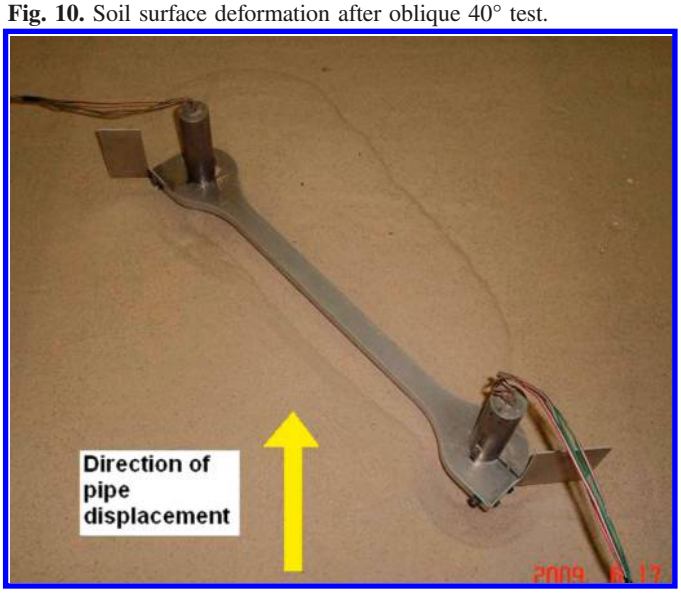

Fig. 11. Numerical versus experimental curves for oblique 70° test.

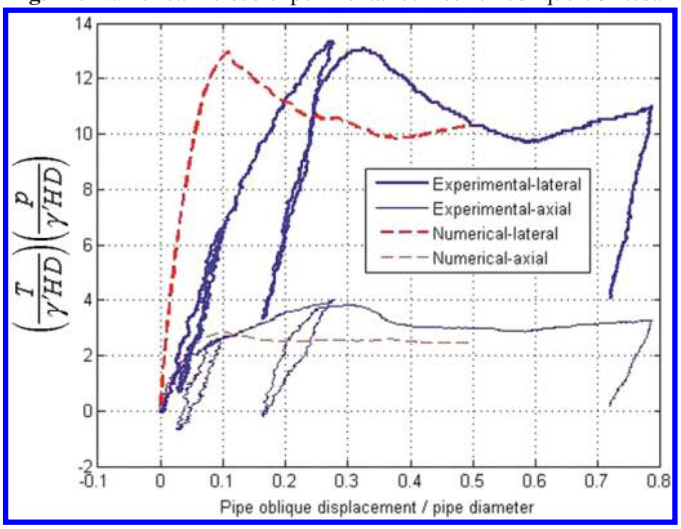

Fig. 12. Numerical versus experimental curves for oblique 40° test.

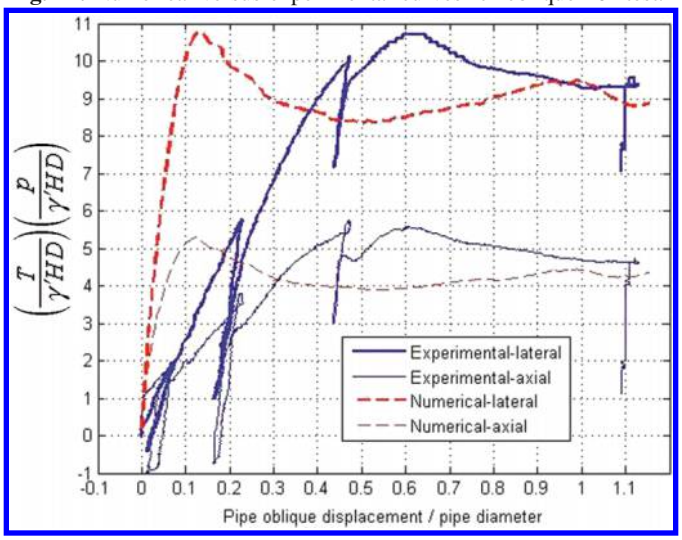

Fig. 13. Comparison of failure mechanisms observed at (*a*) the end of physical modeling versus (*b*) calculated in numerical modeling for oblique 40° test (both in oblique plane).

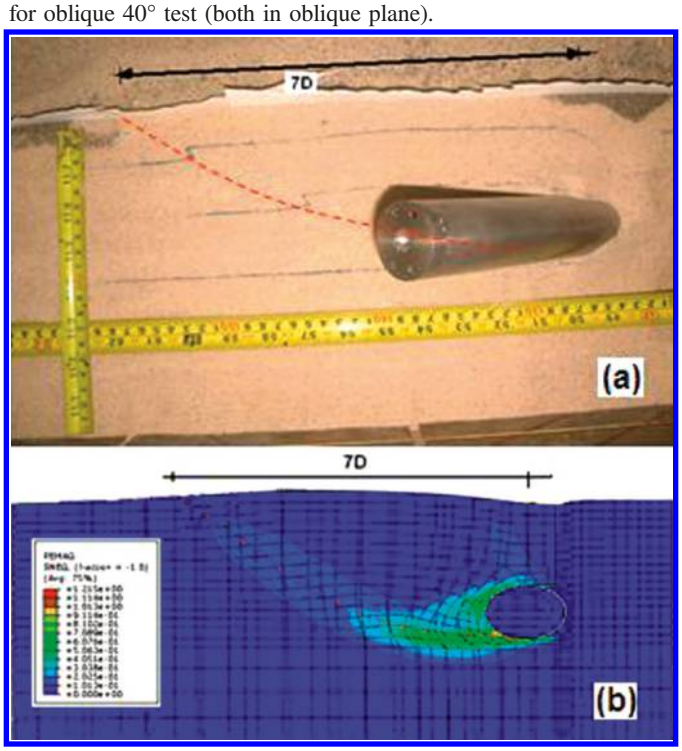

This approach estimates bearing capacity factors (i.e., N_{qh} = 21 for H/D = 2 and φ' = 43°) that are significantly higher than those suggested by other studies. For example, Trautmann (1983) experimental results were consistent with the Ovesen (1964) theoretical model, with estimates of N_{qh} = 8.5 for the same conditions.

Guo and Stolle (2005) have compared several experimental studies on lateral pipe–soil interaction in sand and shown that scale effect has a major influence on the estimated interaction factors. Another important parameter is the vertical restraint. In both the Hansen (1961) theoretical study and Audibert and Nyman (1977) experimental investigation, the vertical movement of pipe was restrained. In the Trautmann (1983) and Ovesen (1964) studies, however, the pipe was free to move vertically during the imposed lateral displacement. Trautmann (1983) suggested that the vertical restraint can double the pipe load.

In addition, for typical pipeline systems, the pipe self-weight is not significant in comparison with the soil self-weight. Trautmann (1983) demonstrated that if the model pipe and loading system are relatively heavy, whereby the model weight becomes a significant fraction of the weight of the soil passive wedge in front of the pipe, the normal stress on the failure surface will increase and result in higher pipeline loads during the test.

In this study, the centrifuge model pipe and support system (i.e., stanchions and dog bone) weight, as shown in Figs. 2 and 3, was about eight times higher than that of an oil-filled pipe at prototype scale. Although vertical motion was unrestrained, the recorded vertical movement was negligible. Numerical simulations that included the effects of pipe self-weight supported this experimental observation, and the estimated peak lateral load (N_{qh} = 13.4) favourably compared

Fig. 14. (*a*) Lateral and (*b*) axial load versus oblique displacement for different oblique angles.

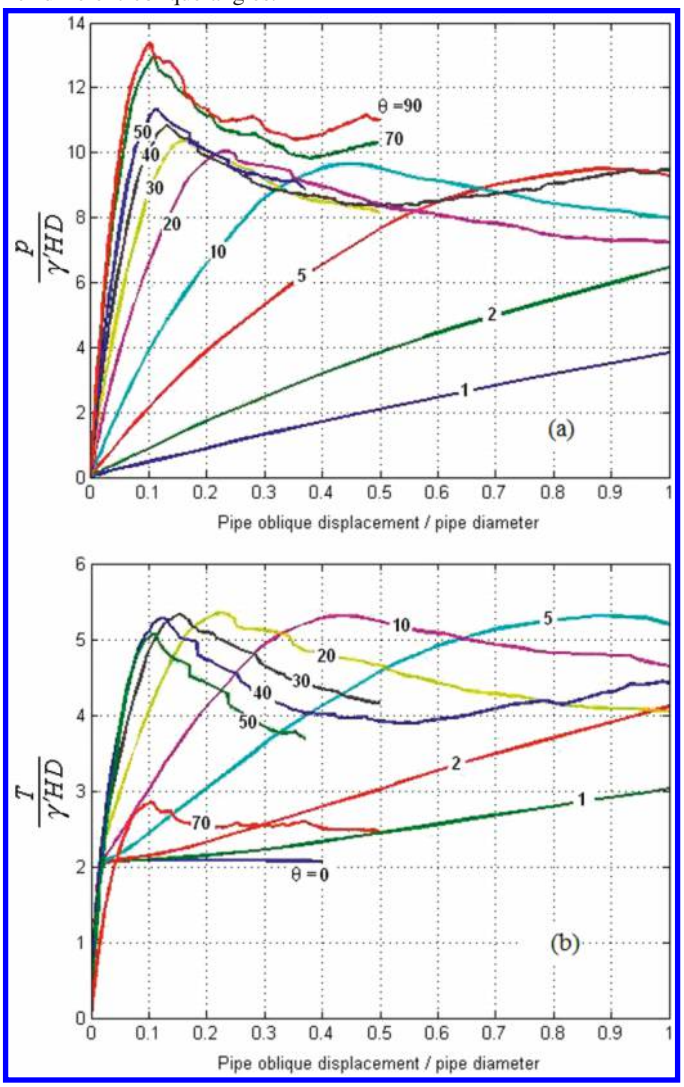

Fig. 15. Variations of lateral and axial interaction factors with oblique angles.

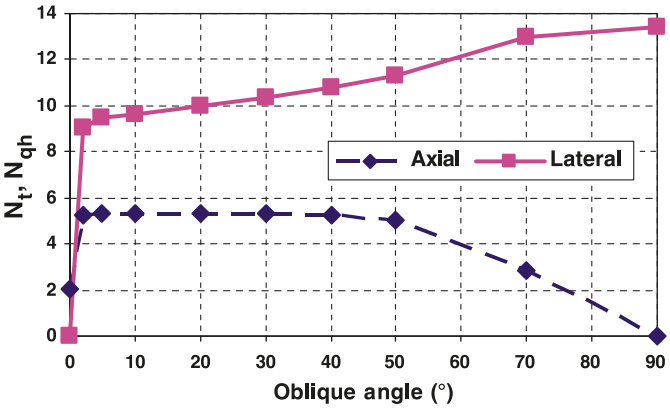

with experimental data. Limit analysis of vertical anchor plates in sand by Merifield and Sloan (2006) resulted in very close lateral bearing capacities to those found in this study ($N_{qh} \approx 14$). This evidence supports the observations of Trautmann (1983) and this study.

Fig. 16. Axial–lateral pipe–soil interaction curves.

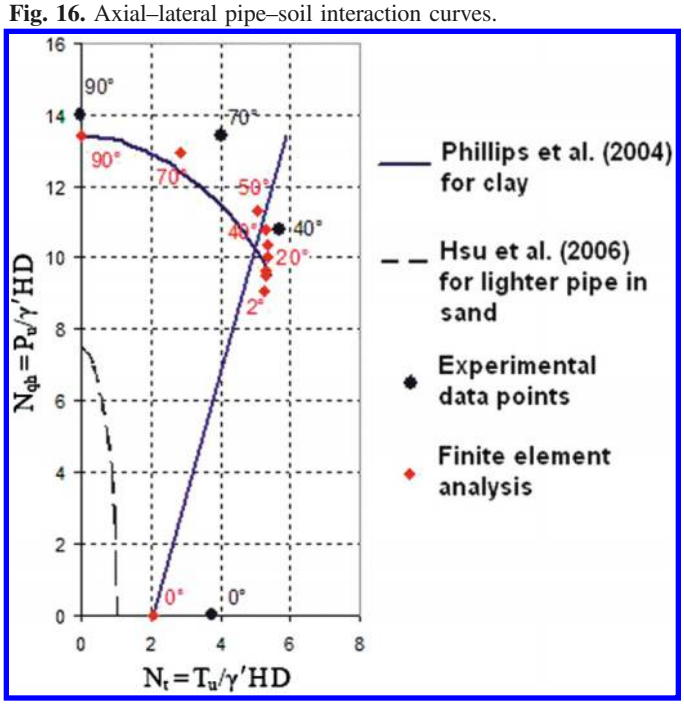

Fig. 17. Mobilization of friction and dilation angles used for parametric studies. ψ_1, ψ_2, ψ_3, dilation angles relevant to peak friction angles of 45°, 40°, and 35°, respectively.

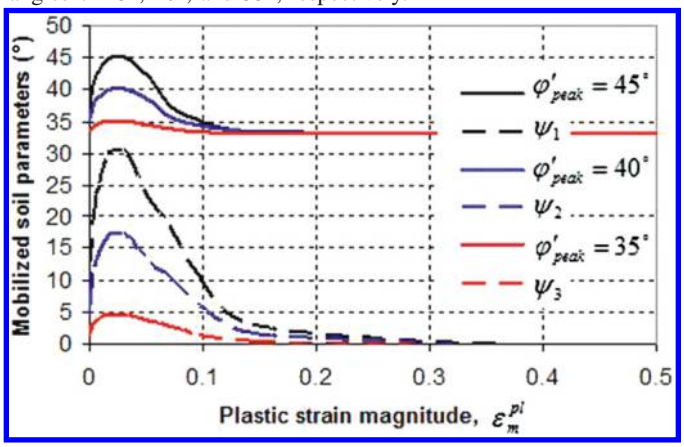

Figure 8 shows the load–displacement curve based on numerical simulation with the same parameters for the results presented in Fig. 7, except for the pipe self-weight. This analysis presented in Fig. 8 would be relevant to a gas-filled steel pipe with a pipe diameter to wall thickness ratio (D/t) of 50, which is about 20 times lighter at prototype scale than the pipe self-weight for the results presented in Fig. 7. The ultimate load from numerical modeling compares very well with the range of ultimate load from Guo and Stolle (2005), which is suggested as

$$[6] \qquad N_{qh} = k\left(\frac{H}{D}\right)^m \left(\frac{D_{ref}}{D}\right)^n$$

where $D_{ref} = 1$ m and for $\varphi' = 43°$; $k = 6$, $m = 0.35$, and $n = 0.2$–0.25.

The ultimate lateral displacement, defined by the lateral displacement to ultimate load, from the centrifuge test ($0.4D$)

Fig. 18. Effect of peak friction angle on axial–lateral pipe–soil interaction.

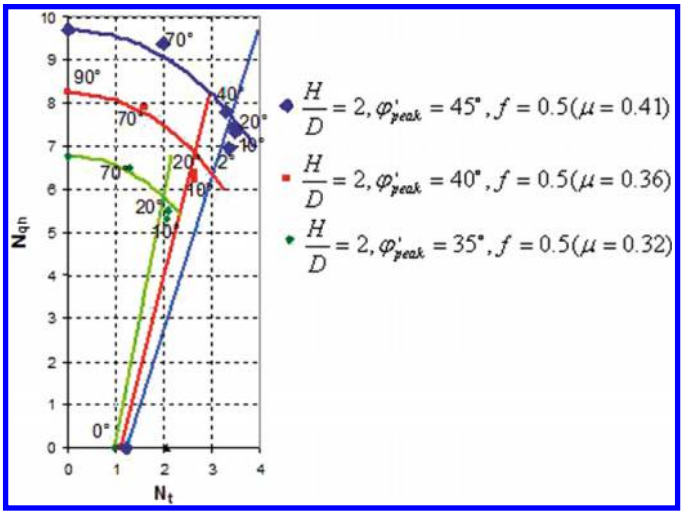

Fig. 19. Effect of interface friction factor on axial–lateral pipe–soil interaction.

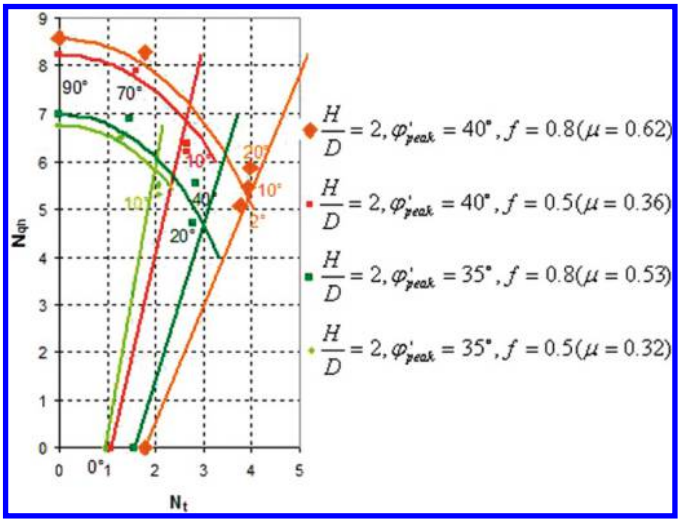

was higher than similar experimental results reported in the literature. The ultimate displacement from Trautmann (1983) large-scale tests was in the range of 0.05–0.075D. Hsu et al. (2006) reported an ultimate displacement of 0.25D for $H/D = 1$ in dense sand during full-scale tests. Dickin (1988) reported ultimate displacements in the range of 0.2D in dense sand during 40g centrifuge tests. This inconsistency between the ultimate displacements in centrifuge tests and 1g tests has been observed in other studies as well.

There may be several reasons that explain this result. Disturbance from test-bed construction (i.e., change in density around pipe during sand pluviation) can cause an effect similar to the trench effect and increase the ultimate displacement during centrifuge tests. The displacements reported from centrifuge tests in this study are also affected by the applied corrections for the actuator compliance. Actuator compliance occurs because of distortion of the rigid frame consisting of pipe, two stanchions, and dog bone (Figs. 2 and 3*b*) in a plane parallel to the direction of movement

Fig. 20. Effect of burial depth on axial–lateral pipe–soil interaction curve.

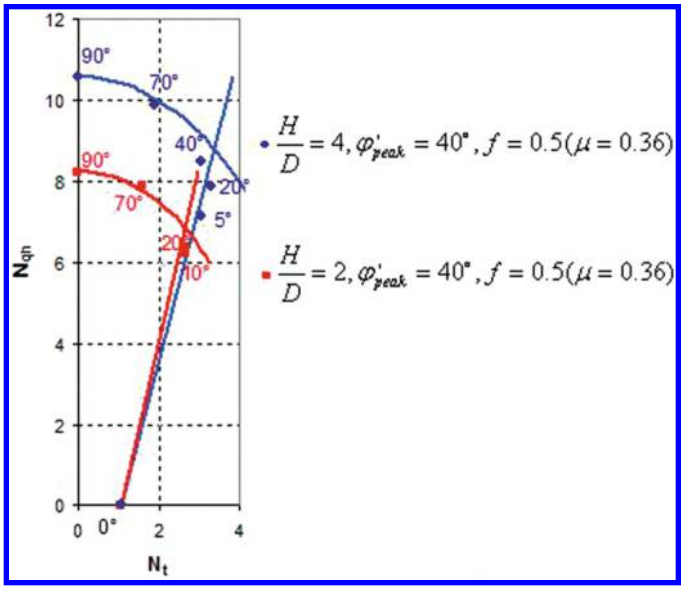

Fig. 21. (*a*) Lateral and (*b*) axial loads versus lateral and axial displacements, respectively, for different oblique angles.

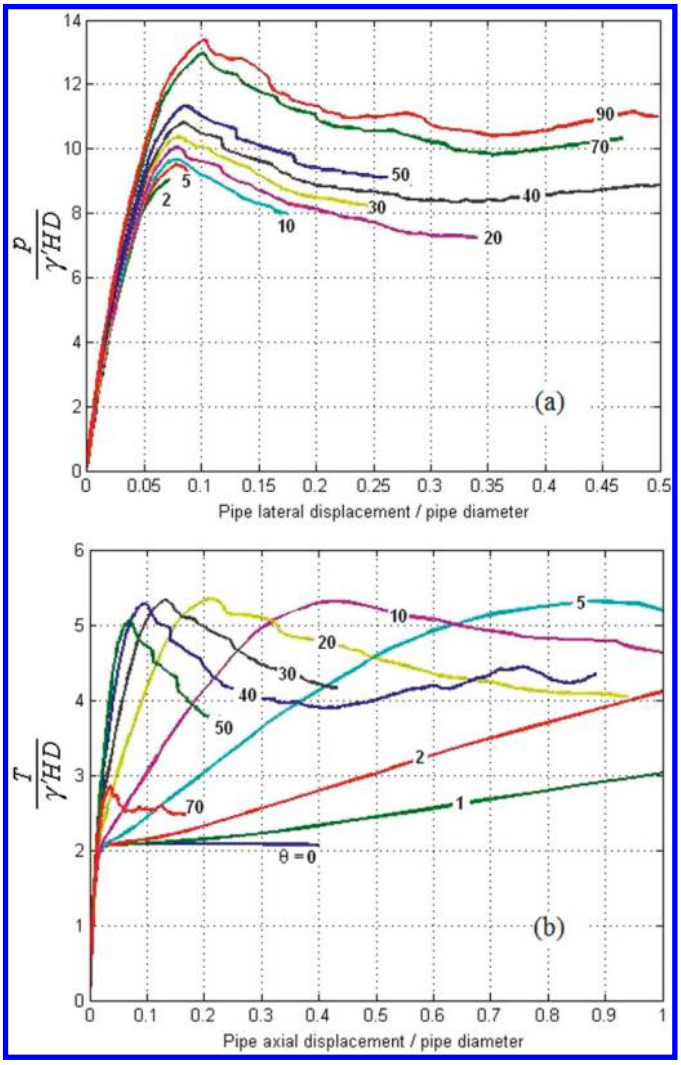

Fig. 22. Ratio of normalized ultimate load over normalized ultimate displacement versus oblique angles.

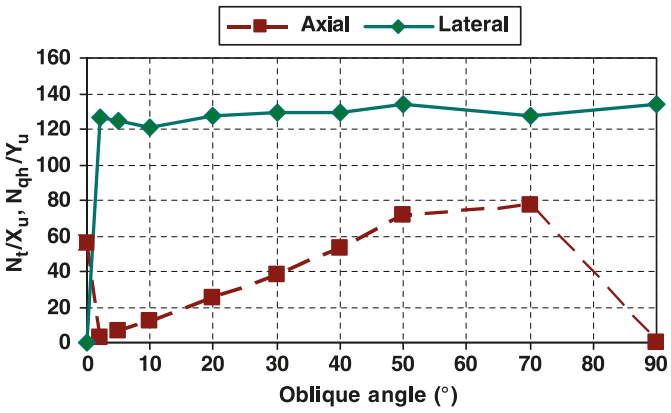

under soil load. This also explains the abnormal shape of the beginning part of the unloading curves. The slopes of the unloading–reloading curves from numerical and experimental modeling, however, are generally consistent.

The ultimate displacement for lateral movement of pipe in sand as recommended by Honegger and Nyman (2004) is defined by

$$[7] \qquad y_u = 0.04(H + D/2)$$

but not more than $0.1D$ to $0.15D$. For $H/D = 2$, this results in $y_u = 0.1D$ and is consistent with the ultimate displacement obtained from numerical analysis in the current study (Fig. 7). For dense sand, a lower value of ultimate displacement has been suggested from other experimental studies (Trautmann (1983) and Audibert and Nyman (1977)):

$$[8] \qquad y_u = 0.02 \sim 0.03(H + D/2)$$

Equation [8] provides a range of $y_u = 0.05 \sim 0.075D$ for $H/D = 2$, which is consistent with a value of ultimate displacement of $0.07D$ from the numerical analysis on the light pipe condition conducted in this study (Fig. 8). Increasing the pipe weight or decreasing the pipe upward movement during lateral pipe–soil relative displacement increases the size of the passive wedge in front of the pipeline. This effect explains the slightly higher lateral displacements required during numerical analysis with heavy pipe (Fig. 7) to reach the ultimate load.

Pure axial loading test

Figure 9 compares the numerical and experimental data for axial pipe–soil interaction, where T is the axial load applied to the unit length of the pipeline. Several unloading–reloading cycles were conducted during the centrifuge test. The experimental load–displacement curve shows the axial interaction factor increases with axial displacement to approximately $0.34D$ (14 mm at model scale). According to Honegger and Nyman (2004), pure axial friction must be mobilized at very small displacements of about 3 mm for dense sand.

The large value for the axial resistance during the centrifuge test can be attributed to a small amount of pipe misalignment in the vertical plane and confined dilation in the sheared sand at the pipe–soil interface. Confined dilation of the sheared sand on the interface increases the normal pres-

sure on the pipe surface, which is equivalent to an increase in the coefficient of lateral earth pressure at rest (K_0), and increases the soil axial restraint on the pipe. Wijewickreme et al. (2009) presented results of full-scale axial tests in dense sand and reported an increase in the axial restraint on the pipeline due to confined shear induced dilation. Also, it is shown later in this paper that a small amount of pipe misalignment in the horizontal plane could cause this kind of increase in the soil axial resistance. These two effects both require larger axial displacements of pipe in the soil than in the case of pure axial friction.

The axial interaction factor is defined as

$$[9] \qquad N_t = T_u/\gamma' HD$$

where T_u is the ultimate axial load.

Honegger and Nyman (2004) suggested the ultimate axial load in cohesionless soils be calculated as

$$[10] \qquad T_u = 0.5\pi D\gamma' H(1 + K_0)\tan\delta$$

where K_0 is the coefficient of lateral earth pressure at rest, and δ is the interface friction angle between soil and pipeline. Equation [10] does not include the pipe self-weight effect, and with a choice of K_0 value of one, results in an axial interaction factor of about 1.4. Schaminee et al. (1990) used the following equation to estimate the axial resistance of a buried pipe, considering the normal stresses on the top, bottom, and sides of an equivalent square:

$$[11] \qquad T_u = 0.25\left[\gamma' H + 2K_a\gamma'\left(H + \frac{D}{2}\right) + \gamma' H + \frac{W_p}{D}\right]\mu\pi D$$

where K_a is the soil active lateral pressure coefficient and W_p is the pipe's self-weight. Using data from Table 2, eq. [11] gives an axial interaction factor of 1.94, which is consistent with the axial interaction factor of 2 from the numerical analysis conducted in the current study (Fig. 9).

Oblique loading

Oblique loading centrifuge tests were conducted for 40° and 70° attack angles. The soil surface deformation at the end of the oblique 40° test is shown in Fig. 10.

Comparisons of numerical and experimental load–displacement curves for oblique 70° and 40° tests are presented in Figs. 11 and 12, respectively. The numerical models have been able to predict the ultimate loads in axial and lateral directions. Discrepancies between the physical data and numerical simulations exist in the estimated ultimate displacements. The contributing factors have been addressed in the section on lateral loading. In comparison with the lateral test condition (Fig. 7), the unload–reload curves from oblique loading tests (Figs. 11 and 12) exhibit improvement. This was due to the addition of two bottom laser displacement sensors (No. 2 in Fig. 3*a*) during the oblique loading tests, which resulted in an improved correction basis for estimating the actuator compliance.

A comparison of the soil failure mechanisms observed at the end of the oblique 40° centrifuge test and predicted by numerical simulation is presented in Fig. 13. The deformation state shown in Fig. 13*b* corresponds to an oblique displacement of 0.6*D*, where numerical model reaches a residual state similar to the end of the physical modeling. Both figures are presented in an oblique plane parallel to direction of pipe movement in the soil. There are similarities in the size of the passive wedge, failure mechanism, and surface heave between the physical and numerical models.

The numerical simulations examined nine oblique angles, including 1°, 2°, 5°, 10°, 20°, 30°, 40°, 50,° and 70°, which are presented in Figs. 14*a* and 14*b*. For oblique 1°, the load–displacement curve is reported for a relative displacement of one pipe diameter, which is less than the ultimate displacement. In this study, loads and displacements corresponding to peak loads are used as ultimate loads and ultimate displacements. To reach the peak axial and lateral loads on the pipe for small oblique angles, larger relative displacements (in terms of several pipe diameters) between pipe and soil are required, which is likely to occur during large ground deformation incidents. The corresponding axial and lateral interaction factors are presented in Fig. 15.

By increasing the oblique angle (i.e., increasing the lateral component of displacement), the lateral load on the pipeline increases (Figs. 14*a*, 15). The axial load increases with increasing oblique angle of attack due to increased axial frictional force related to the increased normal or lateral pressure. For oblique angles larger than 40°, the failure mechanism changes from axial sliding on the pipe surface to shear in the soil mass. Increasing the oblique angle of attack to 90° (i.e., pure lateral loading) decreases the axial restraint on the pipe to zero.

A summary of experimental and numerical ultimate loads is presented in Fig. 16. The interaction curves defined by Phillips et al. (2004) for clay and Hsu et al. (2006) for sand are also shown for comparison. The results indicate that for misalignment less than 40°, the axial force increases by a factor of 2.5. In the centrifuge test for pure axial (0°) loading, the higher axial resistance may be attributed to small misalignment in the vertical plane.

The experimental and numerical data, from this study, support the failure criterion proposed by Phillips et al. (2004). The failure criterion consists of a linear part, associated with soil failure on the pipe circumference, and a nonlinear portion associated with failure through the soil mass. For this study, the transition between the linear and nonlinear components of the failure surface occurred at an oblique angle of approximately 40°. As shown later in this paper, this transition angle was independent of soil friction angle, burial depth, and pipe–soil interface friction for the same soil type.

Honegger et al. (2010) has referred to a similar series of centrifuge tests on sand with lower relative density and saturated clay that yielded similar results to Phillips et al. (2004) and to the current study. The equation of the curved part in Fig. 16 is

$$[12] \qquad N_{qh}^2 + 3N_t^2 = N_{qh(90)}^2$$

where $N_{qh(90)}$ is the ultimate lateral interaction factor during pure lateral pipe–soil relative movement. The linear part connects the point associated with the pure axial condition to a point with horizontal coordinate of (μN_{qh}) and vertical coordinate of (N_{qh}).

Figures 14 and 15 show that applying a small amount of lateral displacement to an axially loaded pipe (even an oblique angle of 1°) will increase the axial soil restraints on the

pipe by a factor of 2.5. This increase has not been considered in current engineering guidelines. In current engineering practice, it is assumed that the maximum axial load on the pipe occurs during pure axial loading, while Figs. 14–16 show, for a wide range of oblique angles, the axial soil restraint on the pipeline is more than pure axial condition. This can be particularly important where upheaval buckling occurs or in other pipe–soil interaction events where axial soil forces play a significant role in the physical mechanisms.

The structural (beam–spring) model is a practical approach used in the pipeline industry particularly when long lengths of pipelines are involved. The interaction curves such as presented in Fig. 16 can be used to define the coupling effects for axial and lateral loading within a beam–spring engineering model simulating pipeline–soil interaction events. Depending on the angle of movement, the ultimate soil restraints in axial and lateral directions can be determined from interaction curves (or semiempirical equations). These ultimate values can be used to define the coupled load–displacement relationships for soil springs (eq. [1]).

Parametric studies have been conducted to obtain a better understanding of the dependence of the interaction curve presented in Fig. 16 on soil properties and important geometrical parameters such as burial depth (H/D). A pipe with a D/t ratio of 50, burial depth ratio (H/D) of 2, and pipe surface friction factor of $f = \delta/\varphi = 0.5$ was examined. Three peak friction angles of 35°, 40°, and 45° were investigated. The hardening law, presented in Fig. 6, was modified in accordance with the corresponding peak friction angles as shown in Fig. 17. As the friction angle increases, the yield surface expands in an approximately linear relationship with increasing friction angle (Fig. 18).

The effect of pipe external coating roughness on the axial–lateral interaction curves is shown in Fig. 19. Two different friction factors of 0.5 and 0.8 are used to simulate pipelines with smooth (e.g., polyethylene) and rough (e.g., steel) external surfaces, respectively. For constant soil parameters and geometrical conditions, increasing the pipe surface friction factor from 0.5 to 0.8 (60% increase) increases the axial load on the pipeline by almost the same percentage for oblique angles lower than 40°. For small oblique angles, increasing the axial component of the load on the pipeline decreases the lateral component of the load according to eq. [12], while the lateral interaction factor for pure lateral movement ($N_{qh(90)}$) slightly increases by increasing the roughness of the pipe external surface. For higher oblique angles, the small amount of increase in the axial component of the load on the pipeline is proportional to the increase in the lateral component of the load. These observations provide confirmation on the two failure mechanisms at lower and higher oblique angles.

Figure 20 presents the effect of burial depth on axial–lateral pipe–soil interaction. Increasing pipe burial depth causes an increase in the axial interaction factor due to higher lateral pressure (i.e., lateral interaction factor) during oblique movements. It is expected that further increase in the interaction factors with burial depth ratio will be limited by a critical depth, where the lateral shear failure mechanism changes to a flow around mechanism.

For all cases presented in Figs. 18–20, the proposed interaction curves match the numerical data points. These figures show that the transition between linear and nonlinear parts of the interaction curves occurs at an oblique angle of approximately 40°. This transition angle is probably a function of soil type and soil state but probably does not vary significantly with changes in soil strength parameters such as the friction angle, pipe–soil interface friction, and pipe burial depth.

Ultimate displacements

While this paper has concentrated on the ultimate loads during oblique movement, proper estimation of ultimate displacements bears the same significance for defining reliable soil spring stiffness terms or material model parameters for macroelements (e.g., Cocchetti et al. 2009). The normalized lateral and axial loads are shown in Figs. 21*a* and 21*b*, respectively, as a function of the normalized lateral and axial displacements for the same cases presented in Fig. 14. The ratio of normalized ultimate load to normalized ultimate displacement are summarized in Fig. 22 for the oblique angles shown in Fig. 21. These data provide a measure of soil spring stiffness.

In the lateral direction, the soil ultimate loads and displacements increase with increasing oblique angle, while the slope of the load–displacement curve remains almost constant (Fig. 22). In the axial direction, excluding the case of pure axial loading, the soil ultimate displacement decreases by increasing the oblique angle. A more complex load–displacement relationship should be developed for the axial direction. The bilinear relationship does not provide adequate estimates, particularly for small oblique angles.

Conclusions

In this study, centrifuge and numerical modeling studies have shown that soil load coupling mechanisms during pipe–soil interaction events can be significant. The axial load can increase by a factor of 2.5 for oblique angles less than 40°. The lateral soil loads can be reduced by factors of 0.75 for small oblique loading angles.

The results from this study support and enhance a two-part failure criterion proposed by Phillips et al. (2004). For oblique axial–lateral pipeline–soil interaction events, the failure surface defines soil failure mechanism on the pipeline circumference for lower oblique angles, generally less than 40°, and shear failure mechanisms through the soil at higher oblique angles of attack.

The predicted ultimate loads from numerical simulation were consistent with the centrifuge data. Using heavy pipes during experimental modeling resulted in larger ultimate loads on pipe. The effect of pipe self-weight on ultimate loads on pipeline is shown using numerical modeling and explained. The ultimate displacements from the centrifuge tests were influenced by test-bed preparation; whereas the ultimate displacements predicted by numerical modeling were consistent with existing industry practice guidelines and literature.

Parametric studies were conducted to investigate the effect of soil friction angle, pipe–soil interface friction factor, and pipe burial depth on axial–lateral pipeline–soil interaction. It was shown that increasing soil friction angle and burial depth proportionally increases the lateral and axial interaction factors for all oblique angles. Increasing the pipe external surface friction factor did not affect the axial and lateral friction

factors for higher oblique angles. For lower oblique angles (almost less than 40°), the axial interaction factors increased proportionally with surface friction factor and decreased with the lateral interaction factor. The proposed failure criterion, as defined by eq. [12], fits well with numerical data from various sets of parameters.

These observations raise questions on the adequacy of current structural-based pipeline–soil interaction models to predict behaviour and assess pipeline integrity for specific design conditions. Therefore, investigating the effects of this coupling on the soil deformation and failure mechanism is important. Developing an improved pipe–soil structural system that is able to consider the interaction between the soil restraints on a pipe moving in different directions with respect to the surrounding soil is significant for estimating the ground effect on the pipeline.

The outcomes of this research study are expected to improve the current guidelines and state of practice in designing energy pipelines by improving understanding of soil loads and resistances on pipelines. Better understanding soil behavior reduces uncertainties of design and vulnerability of pipelines and therefore reduces incidents caused by ground movements, resulting in more economic designs for cases where soil provides resistance against pipeline deformation or structural instabilities such as pipe buckling.

Acknowledgements

The authors would like to thank the C-CORE centrifuge lab staff and also to acknowledge program funding through the Natural Sciences and Engineering Research Council of Canada (NSERC) Discovery Grant, NSERC Major Resource Support, MITACS, and C-CORE.

References

American Lifelines Alliance. 2001. Guideline for the design of buried steel pipe. American Lifelines Alliance (ALA), Federal Emergency Management Agency (FEMA), Washington, D.C.

Aubeny, C.P., Han, S.W., and Murff, J.D. 2003. Inclined load capacity of suction caissons. International Journal for Numerical and Analytical Methods in Geomechanics, **27**(14): 1235–1254. doi:10.1002/nag.319.

Audibert, J.M.E., and Nyman, K.J. 1977. Soil restraint against horizontal motion of pipes. Journal of Geotechnical Engineering Division, ASCE, **103**(10): 1119–1142.

Cocchetti, G., di Prisco, C., Galli, A., and Nova, R. 2009. Soil–pipeline interaction along unstable slopes: a coupled three-dimensional approach. Part 1: Theoretical formulation. Canadian Geotechnical Journal, **46**(11): 1289–1304. doi:10.1139/T09-028.

Dickin, E.A. 1988. Stress–displacement of buried plates and pipes. *In* Proceedings of the International Conference on Geotechnical Centrifuge Modeling (Centrifuge 88), Paris, France, 25–27 April 1988. *Edited by* J.F. Corté. A.A. Balkema, Rotterdam, the Netherlands. pp. 205–214.

European Gas Pipeline Incident Data Group. 2005. Gas pipeline incidents. European Gas Pipeline Incident Data Group (EGIG), Groningen, the Netherlands. 6th EGIG Report 1970–2004, No. EGIG 05-R-0002.

Guo, P., and Stolle, D.F. 2005. Lateral pipe–soil interaction in sand with reference to scale effect. Journal of Geotechnical and Geoenvironmental Engineering, **131**(3): 338–349. doi:10.1061/(ASCE)1090-0241(2005)131:3(338).

Hansen, J.B. 1961. The ultimate resistance of rigid piles against transversal forces. Danish Geotechnical Institute, Copenhagen, Denmark. Bulletin 12, pp. 5–9.

Hibbitt D., Karlsson B., and Sorensen P. 2005. ABAQUS User's Manual. Version 6.5 [computer program]. ABAQUS, Inc., Providence, R.I.

Honegger, D.G., and Nyman, J. 2004. Guidelines for the seismic design and assessment of natural gas and liquid hydrocarbon. Pipeline Research Council International, Falls Church, Va. No. L51927.

Honegger, D.G., Hart, J.D., Phillips, R., Popelar, C., and Gailing, R. W. 2010. Recent PRCI guidelines for pipelines exposed to landslide and ground subsidence hazards. *In* Proceedings of the 8th International Pipeline Conference (IPC2010), Calgary, Alta., 27 September – 1 October 2010. American Society of Mechanical Engineers (ASME), New York. Vol. 2, pp. 71–80.

Hsu, T.W., Chen, Y.J., and Wu, C.Y. 2001. Soil friction resistance of oblique pipelines in loose sand. Journal of Transportation Engineering, **127**(1): 82–87. doi:10.1061/(ASCE)0733-947X(2001)127:1(82).

Hsu, T.W., Chen, Y.J., and Hung, W.Y. 2006. Soil restraint to oblique movement of buried pipes in dense sand. Journal of Transportation Engineering, **132**(2): 175–181. doi:10.1061/(ASCE)0733-947X(2006)132:2(175).

Martin, C.M., and Houlsby, G.T. 2000. Combined loading of spudcan foundation on clay: laboratory tests. Géotechnique, **50**(4): 325–338. doi:10.1680/geot.2000.50.4.325.

Merifield, R.S., and Sloan, S.W. 2006. The ultimate pullout capacity of anchors in frictional soils. Canadian Geotechnical Journal, **43**(8): 852–868. doi:10.1139/t06-052.

Nobahar, A., Popescu, R., and Konuk, I. 2000. Estimating progressive mobilization of soil strength. *In* Proceedings of the 53rd Canadian Geotechnical Conference, Montréal, Que., 15–18 October 2000. *Edited by* D. Leboeuf. BiTech Publishers Ltd., Richmond, B.C.

Nyman, K.J. 1984. Soil response against oblique motion of pipes. Journal of Transportation Engineering, **110**(2): 190–202. doi:10.1061/(ASCE)0733-947X(1984)110:2(190).

Ovesen, N.K. 1964. Anchor slab calculation methods and model tests. Danish Geotechnical Institute, Copenhagen, Denmark. Bulletin 16.

Paulin, M.J., Phillips, R., and Boivin, R. 1995. Centrifuge modeling of lateral pipeline/soil interaction — phase II. *In* Proceedings of the 14th International Conference on Offshore Mechanics and Arctic Engineering (OMAE 95), Copenhagen, Denmark, 18–24 June 1995. *Edited by* S.K. Chakrabarti. American Society of Mechanical Engineers (ASME), New York. Vol. 5, pp. 107–123.

Phillips, R., Nobahar, A., and Zhou, J. 2004. Combined axial and lateral pipe–soil interaction relationships. *In* Proceedings of the International Pipeline Conference (IPC2004), Calgary, Alta., 4–8 October 2004. American Society of Mechanical Engineers (ASME), New York.

Popescu, R., Phillips, R., Konuk, I., Guo, P., and Nobahar, A. 2002. Pipe–soil interaction: large–scale tests and numerical modeling. *In* Proceedings of the International Conference on Physical Modelling in Geotechnics (ICPMG'02), St. John's, N.L., 10–12 July 2002. *Edited by* R. Phillips, P. Guo, and R. Popescu. A.A. Balkema Publishers, Rotterdam, the Netherlands. pp. 917–922.

Schaminee, P.E., Zorn, N.F., and Schotman, G.J.M. 1990. Soil response for pipeline upheaval buckling analyses: full scale laboratory tests and modeling. *In* Proceedings of the 22nd Annual Offshore Technology Conference (OTC6486), Houston, Tex., 7–10 May 1990. American Institute of Mining, Metallurgical, and Petroleum Engineers, Englewood, Colo. pp. 563–572.

Stroud, M.A. 1971. Sand under low stress levels in simple shear apparatus. Ph.D. thesis, Cambridge University, Cambridge, U.K.

Taiebat, H.A., and Carter, J.P. 2000. Numerical studies of the bearing capacity of shallow foundations on cohesive soil subjected to combined loading. Géotechnique, **50**(4): 409–418. doi:10.1680/geot.2000.50.4.409.

Trautmann, C.H. 1983. Behavior of pipe in dry sand under lateral and uplift loading. Ph.D. thesis, Cornell University, Ithaca, N.Y.

Wijewickreme, D., Karimian, H., and Honegger, D. 2009. Response of buried steel pipelines subjected to relative axial soil movement. Canadian Geotechnical Journal, **46**(7): 735–752. doi:10.1139/T09-019.

Yimsiri, S., Soga, K., Yoshizaki, K., Dasari, G.R., and O'Rourke, T. D. 2004. Lateral and upward soil–pipeline interactions in sand for deep embedment conditions. Journal of Geotechnical and Geoenvironmental Engineering, **130**(8): 830–842. doi:10.1061/(ASCE)1090-0241(2004)130:8(830).

List of symbols

c' cohesion
c_u undrained shear strength of soil
D pipe external diameter
D_r relative density
D_{ref} reference diameter
E soil elastic modulus
E_0 soil elastic modulus at reference pressure
F_x ultimate axial force on unit length of pipeline
F_y ultimate lateral force on unit length of pipeline
f pipe surface friction factor
H soil cover depth to the pipe centerline
K_0 coefficient of lateral earth pressure at rest
K_a coefficient of active lateral earth pressure
L pipe length
N_{qh} lateral interaction (bearing capacity) factor
$N_{qh(90)}$ lateral interaction factor for pure lateral pipe–soil interaction
N_t axial interaction factor
N_x axial interaction factor in clay
N_y lateral interaction factor in clay
N_{y90} lateral interaction factor under pure lateral loading
n power exponent
P soil force applied to unit length of pipeline in lateral direction
P_u ultimate (peak) soil force applied to unit length of pipeline in lateral direction
p mean effective stress
p_0 atmospheric pressure
Q soil force applied to unit length of pipeline in vertical direction
q deviatoric stress
T soil force applied to unit length of pipeline in axial direction
T_u ultimate (peak) soil force applied to unit length of pipeline in axial direction
t pipe wall thickness
W_p pipe self-weight
X_u ratio of ultimate relative displacement in axial direction over pipe diameter
x relative displacement in axial direction
x_u ultimate relative displacement in axial direction
Y_u ratio of ultimate relative displacement in lateral direction over pipe diameter
y relative displacement in lateral direction
y_u ultimate relative displacement in lateral direction
z relative displacement in vertical direction
α adhesion factor
γ' effective unit weight of soil
δ interface friction angle between pipeline and soil
$\boldsymbol{\varepsilon}^{pl}$ plastic strain tensor
ε_m^{pl} plastic strain magnitude
θ oblique angle of movement
μ pipe–soil interface friction coefficient
ρ density of soil
φ friction angle
φ' effective friction angle
φ'_{cv} effective constant-volume friction angle
φ'_{peak} effective peak friction angle
ψ dilation angle
ψ_1 dilation angle relevant to peak friction angle of 45°
ψ_2 dilation angle relevant to peak friction angle of 40°
ψ_3 dilation angle relevant to peak friction angle of 35°